

04.2

## The first results of charged fusion product diagnostics at the Globus-M2 spherical tokamak

© N.N. Bakharev<sup>1</sup>, O.M. Skrekel<sup>1</sup>, A.S. Aleksandrov<sup>1</sup>, I.M. Balachenkov<sup>1</sup>, V.I. Varfolomeev<sup>1</sup>, V.K. Gusev<sup>1</sup>, A.N. Kvashnin<sup>2</sup>, V.B. Minaev<sup>1</sup>, Yu.V. Petrov<sup>1</sup>, E.I. Pinzhenin<sup>2</sup>, N.V. Sakharov<sup>1</sup>, A.Yu. Telnova<sup>1</sup>, E.M. Khilkevitch<sup>1</sup>, A.D. Khilchenko<sup>2</sup>, A.E. Shevelev<sup>1</sup>, P.B. Shchegolev<sup>1</sup>, K.D. Shulatiev<sup>1</sup> and Globus-M team<sup>1</sup>

<sup>1</sup> Ioffe Institute, St. Petersburg, Russia

<sup>2</sup> Budker Institute of Nuclear Physics, Siberian Branch of Russian Academy of Sciences, Novosibirsk, Russia

E-mail: bakharev@mail.ioffe.ru

Received May 14, 2024

Revised June 19, 2024

Accepted June 25, 2024

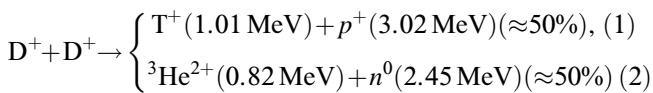
The article presents the first results of applying diagnostics of charged nuclear fusion products at the Globus-M2 tokamak. Specific features of the diagnostics and data obtained are considered. Examples of detector signals and results of their processing are given. A comparison with another diagnostics of nuclear fusion products, namely with the neutron diagnostics, is discussed.

**Keywords:** spherical tokamak, Globus-M2, energetic ions, fusion protons, diagnostics of the charged fusion products.

DOI: 10.61011/0000000000

The nuclear fusion products provide information on spatial distribution of their source which, in its turn, depends on velocity distributions of nuclei participating in the reaction. In small-size tokamaks with low magnetic fields, charged nuclear fusion products with energies of about 1 MeV are not confined in plasma. Due to this, they may be detected and used for the purpose of diagnostics. This article is devoted to the first results of applying the diagnostics of charged fusion products at spherical tokamak Globus-M2 during the 2024 winter-spring experimental campaign.

Nuclear fusion reactions in the Globus-M2 tokamak (major radius of 0.36 m, minor radius of 0.24 m, toroidal magnetic field  $B_T$  of up to 1 T, plasma current  $I_p$  of up to 500 kA) [1] proceed during interaction of fast deuterium ions arising in injecting high-energy atoms with main plasma deuterium ions and with each other:



(here simple estimates of product energies obtained with neglecting kinetic energies of interacting nuclei are considered; an example of calculating energy and angular distributions of fusion products without these neglects can be found in [2,3]). Both branches of this reaction have approximately the same crosssections, and, hence, their probabilities are approximately equal. To make the calculations more accurate, it is possible to use parameterization of differential crosssections proposed in [4]. Most of the produced neutrons leave the tokamak. They are being detected by neutron diagnostic complex [5]. However, complexity of absolute calibration of neutron diagnostics [6], problems with reconstructing the energy and spatial distributions of

neutrons [7], and also high cost of neutron spectrometers make it necessary to use additional diagnostic techniques capable of cross-checking neutron measurements and supplementing them. To this end, diagnostics of charged fusion products may be used.

The charged fusion products diagnostics used in this work consists of semiconductor diode D1 developed at SNIIP-Plus LLC[8], broadband low noise amplifier, and battery power supply. Similar detectors are used in the plasma GDT setup (GDT is the gas-dynamic trap) [9]; this diagnostic technique is described in [10]. In front of the detector, a metal foil was mounted in order to protect the detector against visible range and soft X-ray radiation, as well as against the flux of all the ions and atoms, except for protons of about 3 MeV. In our experiments, steel and molybdenum foils 16 to 30  $\mu\text{m}$  thick and aluminum foil 10 to 42  $\mu\text{m}$  thick were tested. It was found out that a steel or molybdenum foil 16  $\mu\text{m}$  thick is sufficient to completely absorb X-ray radiation, while an incident 3.02 MeV proton loses at it less than half the energy, due to which the useful signal remains significantly above the noise level. Foil of such a thickness does not transmit 1.01 MeV tritons and 0.82 MeV helions, therefore the diagnostics considered here is a detector of fusion protons.

In the experiments, the complex of charged fusion products diagnostics was installed on the only available in this experimental campaign connecting pipe near the equatorial plane at a distance of approximately 1.3 m from the setup axis. The diagnostics coverage areas in discharges with  $I_p = 250 \text{ kA}$  and  $B_T = 0.5, 0.6$  and  $0.7 \text{ T}$  are shown in Fig. 1. To localize those areas, the reverse time motion of the 3.02 MeV hydrogen ions in the tokamak magnetic field was calculated using the orbital code [11]; in simulation, the

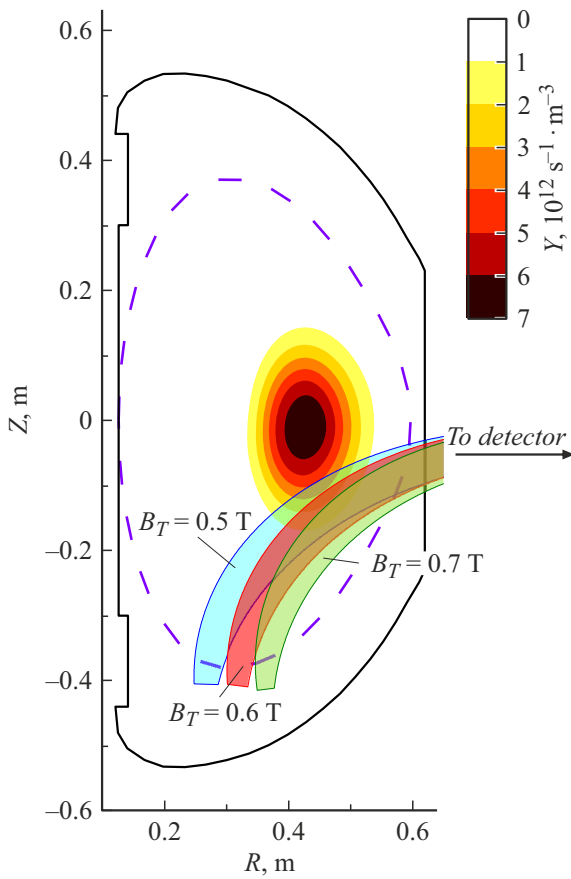


**Figure 1.** Diagnostics coverage area in discharges with plasma current of 250 kA and toroidal magnetic field of 0.5, 0.6 and 0.7 T. The dashed line indicates the last closed magnetic surface; the solid line depicts the chamber wall. The color map represents the characteristic profile of the fusion proton source. The colored figure is given in the electronic version of the article.

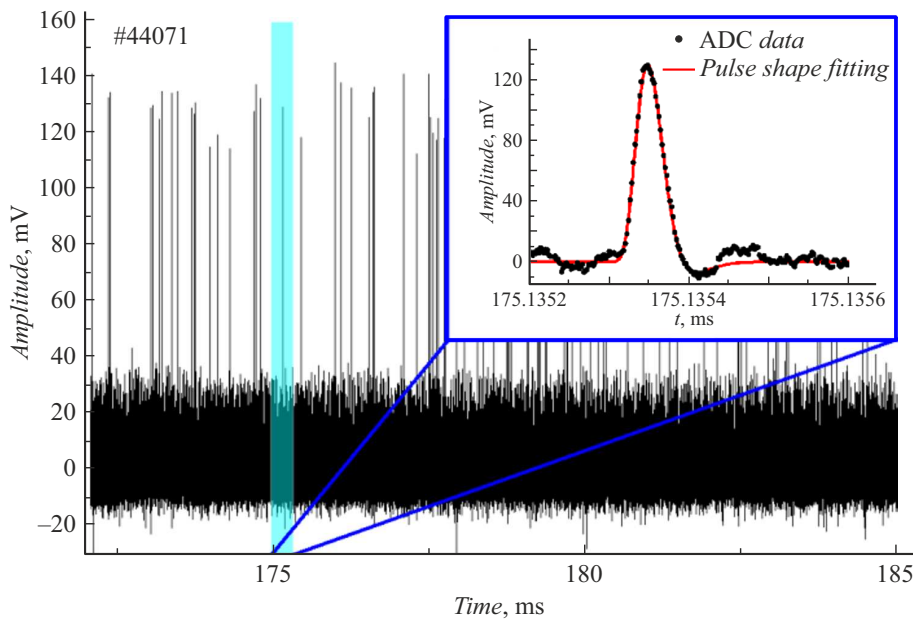
particle starting position was determined by the detector position and dimensions. Areas shown in Fig. 1 differ from each other because of the inversely proportional dependence of the ion Larmor radius on magnetic field. The figure also demonstrates the characteristic profile of the source of fusion protons from the fusion reaction (1) (coinciding with that of the source of neutrons from reaction (2)), which was calculated as described in [11]. Calculations were performed for a discharge with  $I_p = 250$  kA,  $B_T = 0.6$  T and average electron density  $\langle n_e \rangle = 3 \cdot 10^{19} \text{ m}^{-3}$ ; injected particles were deuterium 28 keV in energy, the injection power was 500 kW. As the figure shows, the detector recorded protons generated outside the region with the maximum fusion reaction intensity. The neutron detector coverage area encompasses the entire plasma column; therefore, the neutron detector signal is formed predominantly by neutrons generated in the region with the maximum neutron yield. Because of the difference in measurement areas, the results obtained from the charged fusion product diagnostics supplement the data from the neutron detector.

After the proton is detected, the signal from the detector amplifier is transmitted to 14bit analog-to-digital converter NI PXIe-5164 with the 500 MHz sampling rate. At the amplifier output, each proton registered by the detector relates to a pulse about 150 mV in amplitude (in the case of a molybdenum foil  $30 \mu\text{m}$  thick in front of the detector) and  $< 0.1 \mu\text{s}$  in duration.

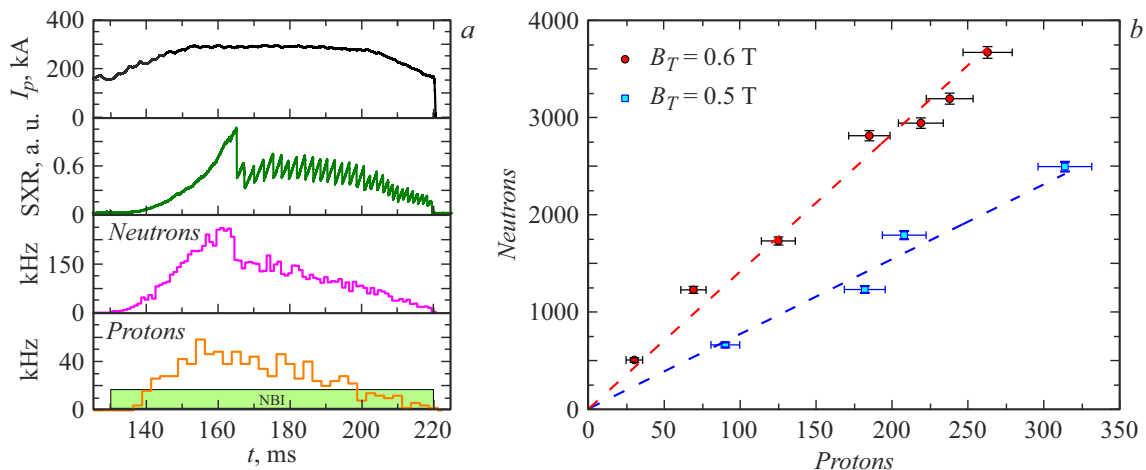
The obtained oscillograms were processed with the algorithm for signal separation based on the pulse shape, which is realized in the DeGaSum code [12]. Using this algorithm instead of the technique of simple threshold discrimination allows separation of pulses superimposed on each other, avoiding detection of false events in the case of emergence of high-amplitude noise, and also more accurate determination of the pulse amplitude and, hence, the detected proton energy. Fig. 2 presents a case of a raw signal from a fusion proton detector in discharge #44071. It also presents a case of measured signal from a separately detected proton and illustrates processing of this event with the DeGaSum code.

Fig. 3, *a* presents a case of processed data obtained using the fusion proton diagnostics in discharge #44116. The toroidal magnetic field in this discharge was 0.7 T; the average electron density was about  $4 \cdot 10^{19} \text{ m}^{-3}$ . The plot illustrates the time evolution of plasma current  $I_p$ , soft X-ray signal, count rate of the neutron detector based on the BC-501A scintillator, and count rate of the fusion proton detector. Injection of 40 keV deuterium with power of about 700 kW was started at the stage of current ramp up at the moment of 130 ms. As shown in the figure, time dependences representing the evolution of neutron and proton fluxes are similar to each other but still have slight differences. First, detection of protons begins only 6 ms after the start of injection, when  $I_p$  reaches 200 kA. This is due to the fact that in the vicinity of the plasma boundary, where a significant part of the proton detector signal comes from, injected fast particles get lost at low  $I_p$ . The losses occur in a short time because of collisions between ionized atoms and tokamak wall (the so-called first-orbit losses) [13]. Second, the proton detector signal stops growing at 155 ms, which is approximately 6 ms earlier than the end of growth of the neutron detector signal. This feature is associated with the fact that the fast ion deceleration time in the center, where a significant part of detectable neutrons are generated, is approximately 2 times higher than in the more peripheral region, where the detectable fusion protons are generated. This is why the fast ion distribution in the central plasma region gets into equilibrium later than at the periphery. Third, the neutron signal decreases sharply at 164 ms. The reason for this decrease is redistribution of fast and thermal ions in the central plasma region during reconnection. The proton detector signal does not exhibit a similar decrease. This is most likely associated with the fact that concentration of ions (both fast and thermal) in the more peripheral region, where the detectable fusion protons are generated, varies insignificantly during reconnection.

In the experiments there was also obtained a dependence of the number of neutrons registered by the detector



**Figure 2.** Raw signal from the fusion proton detector in discharge #44071 and results of using the algorithm for proton signals separation by pulse shape.



**Figure 3.** *a* — discharge #44116 oscillograms. Top to bottom: plasma current, soft X-ray detector signal, neutron detector count rate, proton detector count rate. The rectangle in the bottom panel indicates the time interval during which high energy atoms were being injected. *b* — dependence of the number of detected neutrons on the number of detected protons for two magnitudes of the toroidal magnetic field. Error bars correspond to one standard deviation under the assumption that detected protons and neutrons follow the Poisson distribution.

based on the BC-501A scintillator on the number of protons registered by the diagnostics of fusion protons in discharges with  $B_T = 0.5$  and  $0.6$  T. This dependence is presented in Fig. 3, *b*. The discharge plasma current was  $250$  kA. Each point of the curve corresponds to the number of particles detected in the same discharge in the interval of  $130$  to  $180$  ms. The fusion reaction rate was varied by simultaneously varying the injection energy and power from  $30$  to  $40$  keV and from  $300$  to  $700$  kW, respectively. As the figure shows, the dependence obtained in the experiment for each value of  $B_T$  was linear, which most likely means that the profile of the fusion protons

source changes only slightly with gradually increasing the injection energy from  $30$  to  $40$  keV. The difference in the slopes of the linear dependences is explained by changes in the region wherefrom the protons enter the detector (Fig. 1).

Thus, the diagnostics of charged fusion products was successfully tested at the Globus-M2 tokamak. In the next experimental campaign, we will change the diagnostics complex arrangement in order to increase the proton flux to the detector. Later we are going to consider the possibility of mounting several fusion proton detectors for the purpose of restoring the spatial distribution of fusion proton source.

## Acknowledgements

The work was carried out at the Unique Scientific Facility „Spherical tokamak Globus-M“, which is incorporated in the Federal Joint Research Center „Material Science and Characterization in Advanced Technology“.

## Funding

The tokamak heating systems were prepared in the framework of State Assignment No. FFUG-2021-0001; the tokamak diagnostic systems were prepared in the framework of State Assignment No. FFUG-2024-0028.

## Conflict of interests

The authors declare that they have no conflict of interests.

## References

- [1] Yu.V. Petrov, V.K. Gusev, N.V. Sakharov, V.B. Minaev, V.I. Varfolomeev, V.V. Dyachenko, I.M. Balachenkov, N.N. Bakharev, E.N. Bondarchuk, V.V. Bulanin, F.V. Chernyshev, M.V. Iliasova, A.A. Kavin, E.M. Khilkevitch, N.A. Khromov, E.O. Kiselev, A.N. Konovalov, V.A. Kornev, S.V. Krikunov, G.S. Kurskiev, A.D. Melnik, I.V. Miroshnikov, A.N. Novokhatskii, N.S. Zhiltsov, M.I. Patrov, A.V. Petrov, A.M. Ponomarenko, K.D. Shulyatiev, P.B. Shchegolev, A.E. Shevelev, O.M. Skrekel, A.Yu. Telnova, E.A. Tukhmeneva, V.A. Tokarev, S.Yu. Tolstyakov, A.V. Voronin, A.Yu. Yashin, P.A. Bagryansky, E.G. Zhilin, V.A. Goryainov, *Nucl. Fusion*, **62** (4), 042009 (2022). DOI: 10.1088/1741-4326/ac27c7
- [2] P.R. Goncharov, *Nucl. Fusion*, **55** (6), 063012 (2015). DOI: 10.1088/0029-5515/55/6/063012
- [3] P.R. Goncharov, N.N. Bakharev, *Plasma Phys. Control. Fusion*, **62** (12), 125016 (2020). DOI: 10.1088/1361-6587/abc08d
- [4] P.R. Goncharov, *Atom. Data Nucl. Data Tabl.*, **120** (1), 121 (2018). DOI: 10.1016/j.adt.2017.05.006
- [5] Yu.V. Petrov, P.A. Bagryansky, I.M. Balachenkov, N.N. Bakharev, P.N. Brunkov, V.I. Varfolomeev, A.V. Voronin, V.K. Gusev, V.A. Goryainov, V.V. Dyachenko, N.V. Ermakov, E.G. Zhilin, N.S. Zhiltsov, S.V. Ivanenko, M.V. Il'yasova, A.A. Kavin, E.O. Kiselev, A.N. Konovalov, S.V. Krikunov, G.S. Kurskiev, A.D. Melnik, V.B. Minaev, A.B. Mineev, I.V. Miroshnikov, E.E. Mukhin, A.N. Novokhatsky, A.V. Petrov, A.M. Ponomarenko, N.V. Sakharov, O.M. Skrekel, A.E. Solomakhin, V.V. Solokha, A.Yu. Telnova, E.E. Tkachenko, V.A. Tokarev, S.Yu. Tolstyakov, E.A. Tukhmeneva, E.M. Khil'kevich, N.A. Khromov, F.V. Chernyshev, A.E. Shevelev, P.B. Shchegolev, K.D. Shulyat'ev, A.Yu. Yashin, *Plasma Phys. Rep.*, **49** (12), 1459 (2023). DOI: 10.1134/S1063780X23601360.
- [6] O.M. Skrekel, N.N. Bakharev, V.I. Varfolomeev, V.K. Gusev, M.V. Ilyasova, A.Yu. Telnova, E.M. Khilkevich, A.E. Shevelev, *Tech. Phys.*, **67** (1), 12 (2022). DOI: 10.21883/TP.2022.01.52526.151-21.
- [7] M.V. Iliasova, A.E. Shevelev, E.M. Khilkevitch, N.N. Bakharev, O.M. Skrekel, V.B. Minaev, D.N. Doinikov, D.B. Gin, V.K. Gusev, V.A. Kornev, V.O. Naidenov, A.N. Novokhatskii, Yu.V. Petrov, I.A. Polunovsky, N.V. Sakharov, P.B. Shchegolev, A.Yu. Telnova, V.I. Varfolomeev, *Nucl. Instrum. Meth. Phys. Res. A*, **1029**, 166425 (2022). DOI: 10.1016/j.nima.2022.166425
- [8] <https://sniipplus.ru/>
- [9] P.A. Bagryansky, V.V. Maximov, E.I. Pinzhenin, V.V. Prikhodko, *Fusion Sci. Technol.*, **59** (1T), 256 (2011). DOI: 10.13182/FST11-A11627
- [10] E.I. Pinzhenin, V.V. Maksimov, *PTE*, № 2, v pechati (2024). (in Russian)
- [11] N.N. Bakharev, F.V. Chernyshev, P.R. Goncharov, V.K. Gusev, A.D. Ibyaminova, V.A. Kornev, G.S. Kurskiev, A.D. Melnik, V.B. Minaev, M.I. Mironov, M.I. Patrov, Yu.V. Petrov, N.V. Sakharov, P.B. Shchegolev, S.Yu. Tolstyakov, G.V. Zadvit'skiy, *Nucl. Fusion*, **55** (4), 043023 (2015). DOI: 10.1088/0029-5515/55/4/043023
- [12] O.M. Skrekel, N.N. Bakharev, V.K. Gusev, E.O. Kiselev, *Tech. Phys. Lett.*, **47** (2), 177 (2021). DOI: /10.1134/S1063785021020280.
- [13] E.M. Khilkevitch, A.E. Shevelev, I.N. Chugunov, M.V. Iliasova, D.N. Doinikov, D.B. Gin, V.O. Naidenov, I.A. Polunovsky, *Nucl. Instrum. Meth. Phys. Res. A*, **977**, 164309 (2020). DOI: 10.1016/j.nima.2020.164309

*Translated by EgoTranslating*